Use of U-shaped Donor-Bridge-Acceptor Molecules To Study Electron Tunneling through Nonbonded Contacts

Andrew M. Napper,[†] Nicholas J. Head,[§] Anna M. Oliver,[§] Michael J. Shephard,[§] Michael N. Paddon-Row,*,[§] I. Read,[‡] and David H. Waldeck*,[‡]

Contribution from the Department of Math and Science, Chadron State College, Chadron, Nebraska 69337, Department of Chemistry, University of Pittsburgh, Pittsburgh, Pennsylvania 15260, and Department of Chemistry, University of New South Wales, Sydney, NSW 2052, Australia

Received January 23, 2002

Abstract: A systematic determination of electronic coupling matrix elements in U-shaped molecules is demonstrated. The unique architecture of these systems allows for the determination of the electronic coupling through a pendant molecular moiety that resides between the donor and acceptor groups; this moiety quantifies the efficiency of electron tunneling through nonbonded contacts. Experimental electron-transfer rate constants and reaction free energies are used to calibrate a molecular-based model that describes the solvation energy. This approach makes it possible to experimentally determine electronic couplings and compare them with computational values.

Introduction

Electron transfer is a fundamental chemical process of immense scientific and technological importance. Consequently, it has received much attention.[1] This study evaluates the electron tunneling efficiency between electron donor and acceptor groups by way of noncovalent molecular contacts. The tunneling efficiency is quantified by the electronic coupling matrix element, $|V|$, which characterizes the electronic interaction between an electron donor (D) and acceptor (A). Donor-bridge-acceptor (DBA) molecules have been successfully used to address important issues in electron transfer because they provide systematic control over molecular properties such as bridge geometry,[2] electronic state symmetry,[3] reaction free energy,[4] and others. Electron transfer in DBA molecules can be viewed as a superexchange mechanism that occurs through the orbitals of the intervening medium along a path between the donor and acceptor groups.[5] Recent studies have demon-

strated significant electronic couplings mediated through covalent bonds,[6] through hydrogen bonds,[7] and through solvent molecules.[8,9] This work quantifies the electronic coupling through molecular moieties in van der Waals contact.

The U-shaped DBA systems designed by the Zimmt[9,10] and Paddon-Row[8,13] groups provide insight into the nature of nonadiabatic electron-transfer processes that involve electron tunneling through solvent molecules. These systems have the

---

* To whom correspondence should be addressed. E-mail: (D.H.W.) dave@pitt.edu; (M.N.P.-R.) M.PaddonRow@unsw.edu.au.

† Chadron State College.

‡ University of Pittsburgh.

§ University of New South Wales.

(1) (a) Balzani, V., Ed. *Electron Transfer in Chemistry*; Wiley–VCH: Weinheim, 2001. (b) Barbara, P. F.; Meyer, T. J.; Ratner, M. A. *J. Phys. Chem.* **1996**, *100*, 13148. (c) Electron Transfer–From Isolated Molecules to Biomolecules. *Adv. Chem. Phys.*; Jortner, J., Bixon, M., Eds.; Wiley: New York, 1999.

(2) (a) Hush, N. S.; Paddon-Row, M. N.; Cotsaris, E.; Oevering, H.; Verhoeven, J. W.; Heppener, M. *Chem. Phys. Lett.* **1985**, *117*, 8. (b) Oliver, A. M.; Craig, D. C.; Paddon-Row, M. N.; Kroon, J.; Verhoeven, J. W. *Chem. Phys. Lett.* **1988**, *150*, 366. (c) Johnson, M. D.; Miller, J. R.; Green, N. S.; Closs, G. L. *J. Phys. Chem.* **1989**, *93*, 1173. (d) Paddon-Row, M. N. *Acc. Chem. Res.* **1994**, *27*, 18.

(3) (a) Zeng, Y.; Zimmt, M. B. *J. Phys. Chem.* **1992**, *96*, 8395. (b) Oliver, A. M.; Paddon-Row, M. N.; Kroon, J.; Verhoeven, J. W. *Chem. Phys. Lett.* **1992**, *191*, 371.

(4) Closs, G. L.; Miller, J. R. *Science* **1988**, *240*, 440.

(5) (a) Newton, M. D. *Adv. Chem. Phys.* **1999**, *106*, 303. (b) Jordan, K. D.; Paddon-Row, M. N. *Chem. Rev.* **1992**, *92*, 395.

(6) (a) Paddon-Row, M. N.; Jordan, K. D. In *Modern Models of Bonding and Delocalization*; Liebman, J. F., Greenberg, A., Eds.; VCH Publishers: New York, 1988; Vol. 6, p 115. (b) Shephard, M. J.; Paddon-Row, M. N., Jordan, K. D. *Chem. Phys.* **1993**, *176*, 289. (c) Paddon-Row, M. N.; Shephard, M. J. *J. Am. Chem. Soc.* **1997**, *119*, 5355.

(7) (a) Roberts, J. A.; Kirby, J. P.; Nocera, D. G. *J. Am. Chem. Soc.* **1995**, *117*, 8051. (b) de Rege, P. J. F.; Williams, S. A.; Therien, M. J. *Science* **1995**, *269*, 1409. (c) LeCours, S. M.; Philips, C. M.; DePaula, J. C.; Therien, M. J. *J. Am. Chem. Soc.* **1997**, *119*, 12578. (d) Arimura, T.; Brown, C. T.; Springs, S. L.; Sessler, J. L. *Chem. Commun.* **1996**, 2293.

(8) (a) Lokan, N. R.; Craig, D. C.; Paddon-Row, M. N. *Synlett* **1999**, 397. (b) Lokan, N. R.; Paddon-Row, M. N.; Koeberg, M.; Verhoeven, J. W. *J. Am. Chem. Soc.* **2000**, *122*, 5075. (c) Koeberg, M.; de Groot, M.; Verhoeven, J. W.; Lokan, N. R.; Shephard, M. J.; Paddon-Row, M. N. *J. Phys. Chem.* **2001**, *105*, 3417. (d) Jolliffe, K. A.; Bell, T. D. M.; Ghiggino, K. P.; Jordan, K.; Langford, S. J.; Paddon-Row, M. N. *Angew. Chem., Int. Ed.* **1998**, *37*, 916. (e) Jolliffe, K. A.; Langford, S. J.; Oliver, A. M.; Shephard, M. J.; Paddon-Row, M. N. *Chem.-Eur. J.* **1999**, *5*, 2518. (f) Bell, T. D. M.; Jolliffe, K. A.; Ghiggino, K. P.; Oliver, A. M.; Shephard, M. J.; Langford, S. J.; Paddon-Row, M. N. *J. Am. Chem. Soc.* **2000**, *122*, 10661. (g) Goes, M.; de Groot, M.; Koeberg, M.; Verhoeven, J. W.; Lokan, N. R.; Shephard, M. J.; Paddon-Row, M. N. *J. Phys. Chem. A* **2001**, *105*, 3417.

(9) Kumar, K.; Lin, Z.; Waldeck, D. H.; Zimmt, M. B. *J. Am. Chem. Soc.* **1996**, *118*, 243.

(10) (a) Kumar, K.; Kurnikov, I.; Beratan, D. N.; Waldeck, D. H.; Zimmt, M. B. *J. Phys. Chem. A* **1998**, *102*, 5529. (b) Read, I.; Napper, A.; Kaplan, R.; Zimmt, M. B.; Waldeck, D. H. *J. Am. Chem. Soc.* **1999**, *121*, 10976. (c) Napper, A. M.; Read, I.; Kaplan, R.; Zimmt, M. B.; Waldeck, D. H. *J. Phys. Chem. B* **2002**, in press.

(11) (a) Kaplan, R.; Napper, A. M.; Waldeck, D. H.; Zimmt, M. B. *J. Am. Chem. Soc.* **2002**, submitted. (b) Kaplan, R.; Napper, A.; Waldeck, D. H.; Zimmt, M. B. *J. Am. Chem. Soc.* **2000**, *122*, 12039. (c) Napper, A. M.; Read, I.; Waldeck, D. H.; Kaplan, R. W.; Zimmt, M. B. *J. Phys. Chem. B* **2002**, in press.

(12) Head, N. J.; Oliver, A. M.; Look, K.; Lokan, N. R.; Jones, G. A.; Paddon-Row, M. N. *Angew. Chem., Int. Ed.* **1999**, *38*, 3219.

(13) Napper, A. M.; Read, I.; Waldeck, D. H.; Head, N. J.; Oliver, A. M.; Paddon-Row, M. N. *J. Am. Chem. Soc.* **2000**, *122*, 5220.

Chart 1
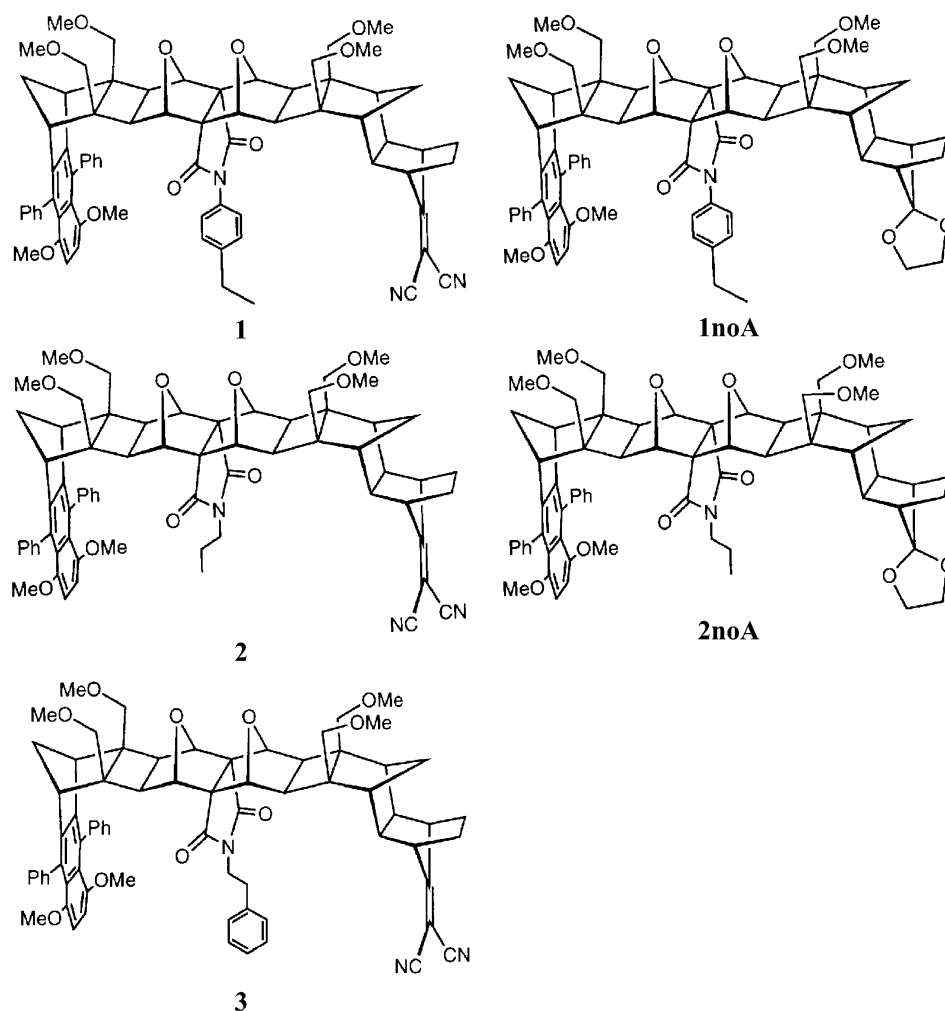
donor and acceptor groups connected by a highly curved, rigid, covalent bridging unit that holds them apart at a fixed distance and orientation. An increase in the electron-transfer rate constant has been observed in such systems when solvents of appropriate sizes and orbital energetics are used. This increase has been ascribed to the occupation of the interior cavity by a solvent molecule(s), for example, benzene or benzonitrile, that allows for an enhanced *line-of-sight* electron tunneling between the donor and acceptor groups, as opposed to a longer, through-bond, coupling pathway occurring via the U-shaped bridge. The electronic couplings determined in these systems can be correlated to the size of the solvent molecule[10b] and its electronic character.[11] However, these systems do not provide direct experimental evidence for the presence of a solvent molecule within the cleft.

More recently, Paddon-Row et al.[12] have constructed supramolecular systems in which a pendant group, covalently attached to the intervening bridge, occupies the interior of the cleft (Chart 1). Comparison of the electron-transfer rates for three different systems, **1**, **2**, and **3**,[13] were measured as a function of solvent polarity. It was shown that when an aromatic moiety is positioned in the *line-of-sight* between the donor and acceptor pair, as in **1**, the observed rate constant is significantly higher than systems in which it is not present, as in **2**, or is not in the *line-of-sight*, as in **3**.[13] The current work quantitatively analyzes the electron-transfer rate data for systems **1** and **2** in

toluene and mesitylene solvents and combines it with earlier data[13] obtained in CH_2Cl_2, THF, and acetonitrile solvents. Electronic structure calculations and the experimental free energies of reaction in the aromatic solvent are used to calibrate a molecular solvation model and subsequently determine the values of the electronic coupling matrix element for **1** and **2**. The electronic couplings are then compared with those calculated for a model system.

A frequently applied analysis of the electron-transfer rate constant relies upon a semiclassical version of the Marcus expression. In this treatment, the solute high-frequency intramolecular degrees of freedom, which are coupled to the charge separation process, are treated as a single effective quantum vibrational mode, and the low-frequency intramolecular and solvent modes are treated classically, so that the rate constant can be expressed as

$$k_{eT} = \frac{2\pi |V|^2}{\hbar \sqrt{4\lambda_o \pi k_B T}} \sum_{n=0}^{\infty} e^{-S}\left(\frac{S^n}{n!}\right) \exp\left[\frac{-(\Delta_r G + \lambda_o + nh\nu)^2}{4\lambda_o k_B T}\right] \quad (1)$$

where $\Delta_r G$ is the reaction free-energy, λ_o is the outer-sphere (solvent) reorganization energy, ν is the frequency of the effective vibrational mode, and S is the Huang–Rhys factor given as the ratio of the inner-sphere reorganization energy, λ_i, to the quantized mode energy spacing, $(\lambda_i/h\nu)$.[1b] The electron-

Chart 2

4 R = H
5 R = Me
6 R = *n*-Pr
7 R = Ph
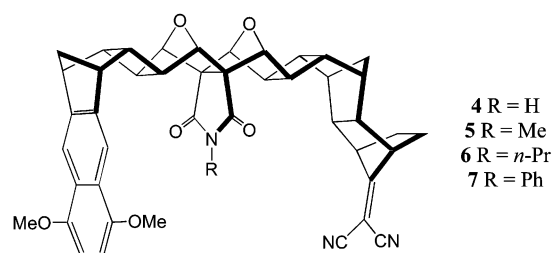
transfer rate constants predicted by eq 1 are a strong function of the parameter set used, and an accurate determination of these parameters is necessary when drawing comparisons with experimental rate data. The quantities $h\nu$ and λ_i are typically evaluated using a combination of experimental charge-transfer spectra and ab initio calculations. Usually, $\Delta_r G$ is estimated through experimental redox data and dielectric continuum corrections to the solvation energy. This approach is not appropriate in weakly polar and nonpolar solvents, however. In this study, $\Delta_r G$ is obtained in nonpolar aromatic solvents from an analysis of the kinetic data using a two-state model. The model assumes that an equilibrium exists between the locally excited state and the charge-separated species and permits evaluation of the forward and backward electron-transfer rate constants. These data are used to calibrate a molecular-based solvation model[14,15] that is able to reproduce the experimental $\Delta_r G(T)$ values. The same model is used to predict the temperature dependence of λ_o. The electronic coupling $|V|$ and $\lambda_o(295$ K) are obtained by fitting the experimental rate constant data using the $\Delta_r G$ and $d\lambda_o/dT$ values from the model in conjunction with λ_i and ν values taken from charge-transfer spectra.[10a,16]

Experimental and Computational Details

Time-resolved fluorescence kinetics of **1** and **2** were measured in toluene and mesitylene as a function of temperature. Comparison of the fluorescence decay kinetics with that of the donor-only reference molecules (**1noA** and **2noA**) allowed the electron-transfer rate constants to be obtained. In all cases, the molecule's excited decay law was found to be biexponential.[17] This finding is consistent with a small reaction free energy for charge separation, $\Delta_r G$. A previous study[13] measured the electron-transfer kinetics for **1** and **2** in CH_2Cl_2, THF, and acetonitrile. In these three solvents, a single-exponential decay was observed, consistent with a larger reaction driving force. Simple continuum calculations suggest that the increased dipolar nature of these solvents leads to an increase in the magnitude of $-\Delta_r G$.

The preparation of the electron-transfer molecules **1** and **2** was reported previously.[12] The solvents were purified in the manner described previously.[10]

The ground and charge-separated (CS) states of the imido systems **4**−**7** were studied computationally (Chart 2). Ground-state geometries of **4**−**7** were optimized at the RHF/3-21G level, whereas the excited singlet CS states were optimized at the UHF/3-21G level. It has been found that the UHF level of theory provides satisfactory optimized geometries of CS states,[18,19] provided that the CS state is the lowest

Table 1. Selected Data for the Ground and CS States of **4**−**7** and **7**′ Obtained from Geometry Optimizations at the (U)HF/3-21G Level

| system | state | $R_c{}^a$ (Å) | $R_e{}^b$ (Å) | θ^c (deg) | μ (D) | charge | | |
						DMN	DCV	imide^d
4	$^1A'$ ground	10.90	11.43		6.01	0.061	−0.191	−0.377
	$^1A''$ CS	6.50	9.56	38.9	12.84	0.830	−0.726	−0.340
5	$^1A'$ ground	10.78	11.38		5.59	0.059	−0.192	−0.358
	$^1A''$ CS	6.59	9.33	33.4	14.81	0.845	−0.718	−0.324
6	$^1A'$ ground	10.70	11.33		5.25	0.058	−0.192	−0.353
	$^1A''$ CS	9.03	11.02	36.5	30.81	0.906	−0.749	−0.382
7	$^1A'$ ground	10.97	11.45		5.75	0.069	−0.187	−0.394
	$^1A''$ CS	8.75	10.86	34.4	28.64	0.893	−0.751	−0.378
7′	$^1A''$ CS				30.53	0.904	−0.768	−0.381

^{a} The center-to-center separation between the chromophores (see Figure 1). ^{b} The bridge edge-to-edge separation (see Figure 1). ^{c} The degree of pyramidalization of the DCV group (see Figure 1). ^{d} The charge on the R group is also included in the total charge on the imide group.

energy state of that particular state symmetry and multiplicity. As the CS states of **4**−**7** possess $^1A''$ state symmetry, that criterion is satisfied in these molecules. All calculations were carried out using the Gaussian 98 program.[20]
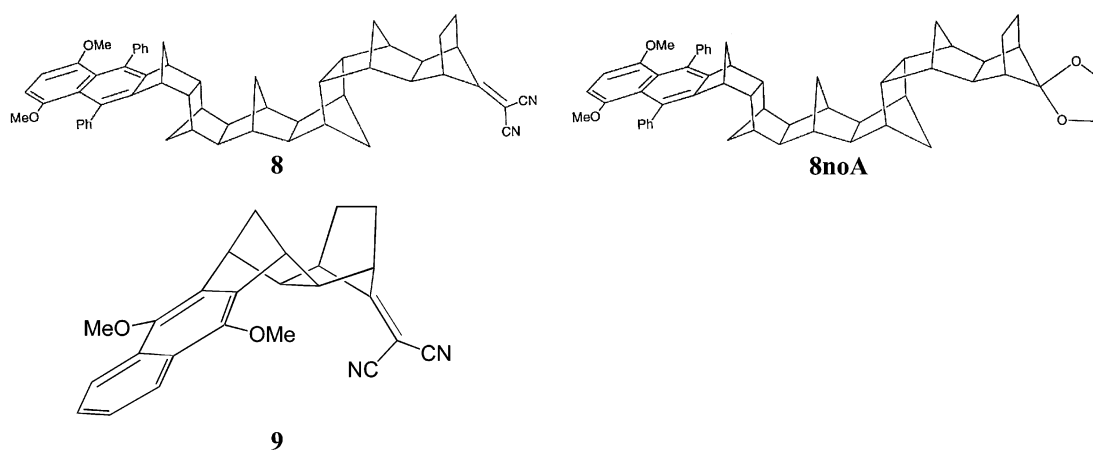
Salient geometric features of the ground and CS states of **4**−**7** are summarized in Table 1. The ground-state geometries for **4**−**7** are all very similar, with the R group only having a small influence (<2%) on the distance between the DMN and DCV groups. The dipole moment varies little (5.3−6.0 D), and the total charges on the DMN, DCV, and imide chromophores show little change in going from **4** to **7**. It should be pointed out that the ground-state optimized geometry of the *N*-phenyl system, **7**, was constrained to have C_s symmetry, with the phenyl ring lying in the plane of the imide group, and hence parallel with the DMN and DCV groups. This is not the global minimum, however; that structure corresponds to the configuration, 1.35 kcal/mol more stable than the C_s structure, where the phenyl ring is rotated 71° out of the imide plane. Similarly, the *N-n*-propyl system, **6**, possesses a global minimum structure similar to, but 0.23 kcal/mol lower in energy than, the C_s symmetric structure used in these calculations. However, because the UHF level geometry optimization calculation of the CS state required that the molecule possess some symmetry, the C_s symmetry structures were used rather than the global minima structures for **6** and **7**.

In general, there is much to criticize in using a single determinant UHF wave function to calculate excited states. Not only does it neglect electron correlation, but it fails to give a qualitatively correct description of the open-shell singlet excited-state wave function − the zeroth-order wave function of such states is biconfigurational. Consequently, the UHF wave function for singlet excited states is severely spin contaminated. Indeed, we find that $\langle S^2 \rangle \approx 1$ for the UHF CS singlet CS states of **4**−**7**, implying ca. 50:50 singlet−triplet mixing. The use of such a low level of theory (UHF) to calculate reliable relaxed geometries and dipole moments (but not energies) of CS states has been addressed and fully justified in earlier publications.[18,19] In particular, we have found that UHF/3-21G optimized geometries and dipole moments for giant CS singlet states related to those studied here are almost the same as those calculated using higher levels of theory, such as CIS which, being multideterminantal, does not lead to spin contamination of the

(14) Read, I.; Napper, A. M.; Zimmt, M. B.; Waldeck, D. H. *J. Phys. Chem. A* **2000**, *104*, 9385.
(15) Matyushov, D. V.; Voth, G. A. *J. Chem. Phys.* **1999**, *111*, 3630.
(16) (a) Marcus, R. A. *J. Phys. Chem.* **1989**, *93*, 3078. (b) Lilichenko, M.; Tittelbach-Helmrich, D.; Verhoeven, J. W.; Gould, I. R.; Myers, A. B. *J. Chem. Phys.* **1998**, *109*, 10958.
(17) As described in an earlier report,[13] the fluorescence decay also shows a contribution from an impurity that corresponds to the donor only compound, but this feature is accounted for in the data fitting.
(18) Shephard, M. J.; Paddon-Row, M. N. *J. Phys. Chem.* **1999**, *103*, 3347.
(19) Shephard, M. J.; Paddon-Row, M. N. *J. Phys. Chem.* **2000**, *104*, 11628.

(20) Frisch, M. J.; Trucks, G. W.; Schlegel, H. B.; Scuseria, G. E.; Robb, M. A.; Cheeseman, J. R.; Zakrzewski, V. G.; Montgomery, J. A., Jr.; Stratmann, R. E.; Burant, J. C.; Dapprich, S.; Millam, J. M.; Daniels, A. D.; Kudin, K. N.; Strain, M. C.; Farkas, O.; Tomasi, J.; Barone, V.; Cossi, M.; Cammi, R.; Mennucci, B.; Pomelli, C.; Adamo, C.; Clifford, S.; Ochterski, J.; Petersson, G. A.; Ayala, P. Y.; Cui, Q.; Morokuma, K.; Malick, D. K.; Rabuck, A. D.; Raghavachari, K.; Foresman, J. B.; Cioslowski, J.; Ortiz, J. V.; Stefanov, B. B.; Liu, G.; Liashenko, A.; Piskorz, P.; Komaromi, I.; Gomperts, R.; Martin, R. L.; Fox, D. J.; Keith, T.; Al-Laham, M. A.; Peng, C. Y.; Nanayakkara, A.; Gonzalez, C.; Challacombe, M.; Gill, P. M. W.; Johnson, B. G.; Chen, W.; Wong, M. W.; Andres, J. L.; Head-Gordon, M.; Replogle, E. S.; Pople, J. A. *Gaussian 98*; Gaussian, Inc.: Pittsburgh, PA, 1998.

Chart 3

molecules. The electron-transfer rate constant of **8** in toluene was found to be less than $2 \times 10^8 \text{ s}^{-1}$ at 293 and 333 K. In contrast, the electron-transfer rate constant of **1** in toluene was found to be $29 \times 10^8 \text{ s}^{-1}$ at 327 K, and the electron-transfer rate constant of **2** in toluene was found to be $16 \times 10^8 \text{ s}^{-1}$ at 327 K. A comprehensive set of electron-transfer rate constant data for **1** and **2** as a function of temperature is provided in the Supporting Information. These data show that in the case of **1** and **2** the through-bond coupling mechanism is only weakly present, having only a minor influence on the overall coupling.

Determination of λ_i and $h\nu$. Charge-transfer absorption and emission band shape analysis provide an effective means of determining the internal reorganization energy associated with the electron donor and acceptor groups. For an electron-transfer reaction that is coupled to a single, effective, high-frequency vibrational mode, the emission band shape $L(\Delta E)$ is given by

$$L(\Delta E) = \exp(-S) \sum_{n=0}^{\infty} \frac{S^n}{n!} \exp\left[-\frac{(\Delta_r G + \Delta E + nh\nu + \lambda_o)^2}{4\lambda_o k_B T} \right]$$

(2)

where ΔE is the photon energy. In practice, the fitting treats $\Delta_r G$, $h\nu$, λ_i, and λ_o as adjustable parameters and often gives several parameter sets that provide adequate fits. By combining this analysis with quantum chemical calculations, a suitable range of parameter values can be established.[10]

Charge-Transfer Spectra. In the present work, the internal reorganization energy is determined using the charge-transfer absorption and emission spectra for a related compound, **9**, in hexane.[21d,22] Although **9** has a different bridge structure than those of **1** and **2**, it has the same donor and acceptor groups and can reliably be used to quantify the internal reorganization parameters, because they are primarily associated with the geometry changes of the donor and acceptor upon electron transfer. The Stokes shift, B, is related to the total reorganization energy through

$$B = 2(\lambda_o + \lambda_i)$$

(3)

and the Stokes shift for **9** in hexane is $B = 1.26$ eV. Assuming that λ_o in this solvent is zero, one obtains a value of 0.63 eV for λ_i. The frequency of the effective quantum mode can be

singlet CS-state wave function. We have also found that, at the UHF, CIS, and DFT levels of theory, triplet CS-state relaxed geometries and dipole moments of a variety of bichromophoric systems reported in ref 18 are practically identical to those calculated for the respective singlet CS states. This finding is not unexpected, given that charge separation is practically complete in the CS states of these giant bichromophoric systems and that the two radical ion chromophores are only *weakly coupled*; that is, the CS states may be regarded as two isolated radical ions interacting almost exclusively by Coulombic attraction. Consequently, both singlet and triplet wave functions are expected to have nearly the same spatial distribution. This explains why − notwithstanding severe spin contamination, amounting to 50: 50 singlet−triplet mixing − the UHF relaxed singlet CS-state geometries and dipole moments should be of acceptable quality. Last, the geometry for **7** was optimized at the CIS/3-21G level and compared to that obtained at the UHF level. The geometry and dipole moments of the CS singlet state are nearly the same in the two calculations. The CIS dipole moment is 28.56 D, as compared to 28.64 D (reported in Table 1). The only noticeable geometric difference is in the pyramidalization angle (θ in Table 1) about the DCV group; at the UHF level, it is 34.4°, whereas at the CIS/3-21G level, it is 28.2°. This discrepancy is quite small and does not impact the conclusions.

Evaluation of Through-Bond Mediated Electron Transfer

Given the U-shaped architecture of molecules **1** and **2**, the intervening pendant group should mediate electron transfer between the donor and acceptor chromophores in preference to the two chromophores, coupling via the orbitals of the connecting bridge in a *through-bond,* or superexchange, mechanism. The through-bond mechanism has been extensively studied in similar systems.[21] The importance of the through-bond coupling mechanism, which may be in operation in **1** and **2**, to the overall electronic coupling was assessed by comparing the electron-transfer rate of **1** and **2** with that of a reference system, **8** (Chart 3). System **8** possesses a bridge with the same number of bonds linking the donor and acceptor chromophores as in molecules **1** and **2**; however, it does not possess the U-shaped architecture, so that the most direct coupling of the donor and acceptor is via the bonds of the bridge and not through any solvent

(21) (a) Warman, J. M.; de Haas, M. P.; Paddon-Row, M. N.; Cotsaris, E.; Hush, N. S.; Oevering, H.; Verhoeven, J. W. *Nature* **1986**, *320*, 615. (b) Penfield, K. W.; Miller, J. R.; Paddon-Row, M. N.; Cotsaris, E.; Oliver, A. M.; Hush, N. S. *J. Am. Chem. Soc.* **1987**, *109*, 5061. (c) Warman, J. M.; de Haas, M. P.; Verhoeven, J. W.; Paddon-Row, M. N. *Adv. Chem. Phys.* **1999**, *106*, 571. (d) Oevering, H.; Verhoeven, J. W.; Paddon-Row, M. N.; Warman, J. M. *Tetrahedron* **1989**, *45*, 4751.

(22) Oevering, H.; Paddon-Row, M. N.; Heppener, H.; Oliver, A. M.; Cotsaris, E.; Verhoeven, J. W.; Hush, N. S. *J. Am. Chem. Soc.* **1987**, *109*, 9, 3258.
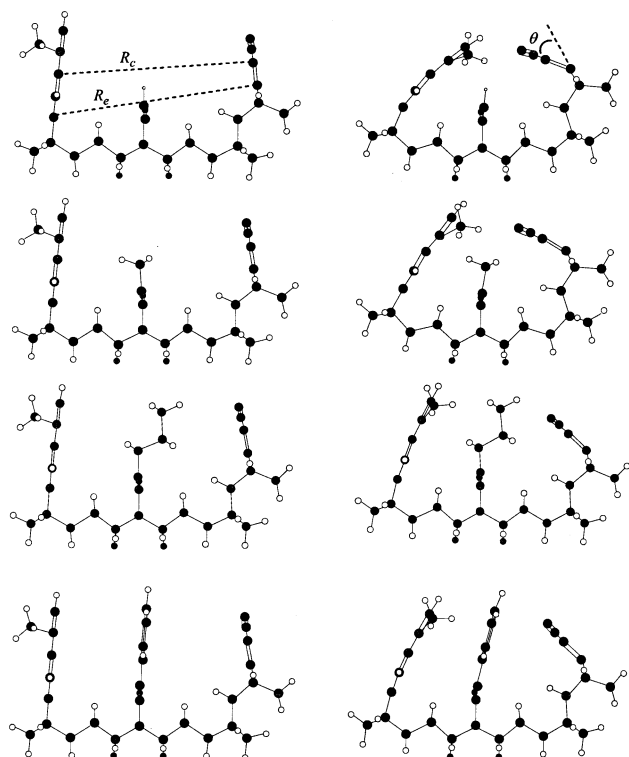
Figure 1. Profiles of the ground (left) and CS (right) optimized geometries for the systems **4** (top)−**7** (bottom) obtained at the (U)HF/3-21G level.

determined from the charge-transfer emission bandwidth, $\Delta E_{1/2}$. When the mode frequency $h\nu \gg k_B T$, the emission bandwidth can be written as

$$(\Delta E_{1/2})^2 \cong 8(\ln 2)(2k_B T\lambda_o + \lambda_i h\langle v\rangle) \qquad (4)$$

Assuming that the outer-sphere reorganization energy is zero in hexane, one finds an average intramolecular mode frequency, $h\langle\nu\rangle$, of 1100 cm^{-1} from the emission spectrum shown in ref 21d.

Theoretical Calculations. Quantum chemical calculations indicate that electron transfer can result in dramatic geometrical changes between the ground and charge-separated states for these U-shaped molecules, particularly in nonpolar solvents.[18,19] The two major structural features present in the CS-state geometries, compared to those calculated for the ground states, are the pyramidalization of the DCV radical anion group at C7 and the degree of distortion in the DMN radical cation group, as shown in Figure 1. Some distortion of the connecting bridge also occurs. While the pyramidalization is inherent in the DCV radical anion species,[18,19] the direction of this pyramidalization and the general distortion of both the DMN group and the bridge arise from the strong Coulomb attraction between the two oppositely charged ends of the molecule. For example, the center-to-center chromophore separation, R_c, contracts, on average, by 3.6 Å, while the bridge's edge-to-edge separation, R_e, contracts by about 1.5 Å (Figure 1 and Table 1). Unlike the ground-state structures, the R_c and R_e values found for the CS-state geometries of **4**−**7** depend on the nature of the imide substituent group, R. For R_c, the range of values for the CS-state geometries is 2.53 Å, whereas for the ground states, it is only 0.21 Å. For R_e, the ranges are 1.69 Å in the CS states and 0.11 Å in the ground state. Especially noticeable is the difference
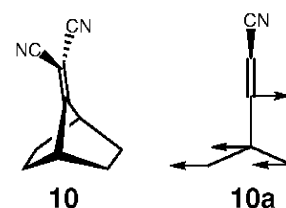
in the R_c distances between the molecules with small pendant groups, **4** (6.50 Å) and **5** (6.59 Å), as compared to the molecules with more bulky pendant groups, **6** (9.03 Å) and **7** (8.75 Å). This difference arises from the size of the *n*-propyl and phenyl groups, which are fully interposed between the DMN and the DCV groups in **6** and **7**, respectively. The steric bulk of these groups forces the oppositely charged DMN$^+$ and DCV$^-$ chromophores in the CS state to remain further apart despite the strong Coulomb attraction. In contrast, the H and methyl groups are small enough to allow significant distortion of the DMN and DCV chromophores to occur. Consequently, the charge-transfer state dipole moment that was calculated for molecule **7** was used in the calculations of the outer-sphere reorganization energy and Gibbs free energy of reaction, which are presented below.

We emphasize that all optimized geometries refer to gas-phase structures. Consequently, the relaxed gas-phase geometries of the CS states will be more distorted than those in solvent because the electrostatic interactions will be attenuated in solvent. Unfortunately, all attempts so far to calculate relaxed geometries by including solvent effects (using solvation continuum models) have failed, owing to the lack of convergence in the SCF part of the calculation. Nevertheless, we did manage to calculate the relaxed geometry for the radical anion of 7-dicyanovinylnorbornane, **10**, in a solvent continuum having a dielectric of 37.5, equivalent to acetonitrile. As with the gas-phase structure, **10** displayed a marked pyramidalization about the DCV group. We therefore believe that our relaxed gas-phase geometries of CS states reveal structural features that are retained, perhaps to an attenuated degree, in solvents.

Two vibrational modes appear to be coupled to the electron transfer in our systems. First, the formation of the anion involves a pyramidalization of the DCV acceptor group and an out-of-plane bending mode (see Chart 4). The frequency associated with out-of-plane bending of the DCV group, schematically depicted by **10a**, is 1088 cm^{-1}.[23] Second, the naphthalene ring undergoes a ring deformation upon formation of the cation that primarily involves stretching modes at ~1600 cm^{-1}. These frequencies bracket the 1100 cm^{-1} effective mode frequency found from the analysis of the charge-transfer spectra. Both results are consistent with the large internal reorganization energy observed in these systems. With no information at this time as to the degree of partitioning of the internal reorganization energy with respect to the high-frequency modes, the analysis is largely limited to the case of a single high-frequency mode of 1600 cm^{-1}. This choice is consistent with prior attempts at

(23) A harmonic frequency calculation was carried out on neutral 7-dicyanovinylnorbornane **10**. The level of theory used was B3LYP/6-311+G(d,p)// B3LYP/6-311+G(d,p), and the geometry optimization was carried out under C_{2v} symmetry constraint. The frequency associated with out-of-plane bending of the DCV group, schematically depicted by **10a**, is 1132 cm^{-1}. Applying the recommended scaling factor of 0.9613 gave a corrected frequency of 1088 cm^{-1}; see: Wong, M. W. *Chem. Phys. Lett.* **1996**, *256*, 391.
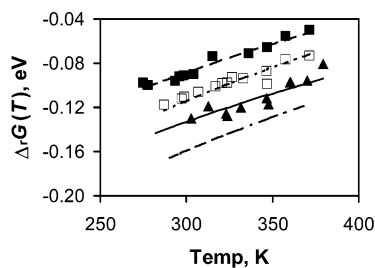
Figure 2. The experimental $\Delta_r G$ values are plotted for **1** in toluene (□) and mesitylene (■). The experimental values for **2** in mesitylene are shown as ▲. The lines show the $\Delta_r G$ values predicted for all four aromatic systems by the molecular model with the parameters given in Table 2. The experimental values for **2** in toluene could not reliably be determined from the fluorescence lifetime data. The $\Delta_r G$ values predicted by the model for **2** in toluene are indicated by the bottom dot−dashed line. See text for details.

analysis using the semiclassical equation in related systems with dicyanoethylene acceptors.[10a] The effect of independently partitioning the inner-sphere reorganization energy between two modes, taken to be 990 and 1600 cm^{-1}, was explored to examine its impact on the ratio of the electronic coupling matrix element for **1** and **2**. Calculations of the actual partitioning of the inner-sphere reorganization energy are underway and will be published later. Last, no matter what partitioning was used, the electronic coupling was always larger for **1** than **2**.

Determination of $\Delta_r G$

$\Delta_r G$ can be determined from experimental fluorescence lifetime data, provided the locally excited (LE) and charge-separated states lie close in energy, so that an excited-state equilibrium occurs.[10b,24,25] The analysis assumes that the absorption and emission of radiation arise from the LE state of the donor and allow the rate constants k_{for} (LE to CS) and k_{back} (CS to LE) to be determined. Their ratio is used to compute $\Delta_r G$. This behavior was observed for **1** in both toluene and mesitylene. In toluene and mesitylene, the reaction free energy for **1** changes systematically with temperature from −0.12 and −0.05 eV (see Figure 2). At higher temperatures, the same effect was observed for **2** in mesitylene. In toluene, the fluorescence lifetime decay was clearly dominated by the short time component (ca. 99% or greater at all the temperatures), so that it was not possible to accurately determine the reaction free energy for this solvent. In the more polar solvents, THF, CH$_2$-Cl$_2$, and CH$_3$CN, the CS state is sufficiently stabilized so that the back electron transfer is not observed.[13]

The measured $\Delta_r G$ values for **1** (in mesitylene and toluene) and **2** (in mesitylene only) were used to calibrate a molecular-based solvation model. The model was then used to predict the temperature dependence of λ_o and the reaction free energy in more polar solvents. The model treats the solute and solvent molecules as polarizable hard spheres and accounts for dipole−dipole, dipole−quadrupole, induction, and dispersion interactions. $\Delta_r G$ is calculated as the sum of four components

$$\Delta_r G = \Delta_{vac} G + \Delta_{dq,i} G^{(1)} + \Delta_{disp} G + \Delta_i G^{(2)} \qquad (5)$$

Table 2. Parameters Used in the Molecular Solvation Model

solute radius (Å)	7.77
$\Delta_{vac}G$ (eV) for **1**	0.159
$\Delta_{vac}G$ (eV) for **2**	0.114
$\Delta\gamma'$ (Å^3)	6.2
μ_{ex} (D)	28.64
μ_{gs} (D)	5.75
toluene polarizability (Å^3)	12.32
mesitylene polarizability (Å^3)	16.14

where $\Delta_{vac}G$ is the free energy of the process in a vacuum, $\Delta_{dq,i}G^{(1)}$ is the contribution from first-order dipole, quadrupole, and induction interactions, $\Delta_{disp}G$ is the contribution from dispersion interactions, and $\Delta_i G^{(2)}$ represents contributions from second-order induction interactions. Details about this model and its implementation are provided in Appendix A and elsewhere.[14]

Use of this model requires parameters for both the solute and the solvent. The toluene and mesitylene solvent parameters are the same as those described in earlier work.[14] The solute ground- and excited-state dipole moments were set equal to those calculated at the UHF/3-21G level for **7** (Table 1), 5.75 D for the ground state and 28.64 D for the CS state. The polarizability was calculated to be ∼128 Å^3 for **1** and 124 Å^3 for **2**.[26] Table 2 summarizes the other solute parameters. Calibration of the molecular model requires determination of the parameters $\Delta_{vac}G$, the solute radius R_o, and $\Delta\gamma'$. The temperature dependent $\Delta_r G$ values in toluene and mesitylene, measured for **1** and **2** (mesitylene only), were simultaneously fit to eq 5 by adjusting these three parameters.

The fit of the model to the experimental $\Delta_r G$ for **1** in toluene, and **1** and **2** in mesitylene, and the predicted $\Delta_r G$ values for **2** in toluene are shown in Figure 2. Given the similarity between molecules **1** and **2**, the parameter set was taken to be the same for both solutes with the exception of $\Delta_{vac}G$. The $\Delta_{vac}G$ value was chosen independently for the two solutes, so that the $\Delta_r G$ value in **2** was more negative than that in **1**, an observation consistent with the experimental data. The difference in $\Delta_{vac}G$ for **1** and **2** can be rationalized as the difference in the Coulomb stabilization energies for **1** and **2** in a vacuum. Using effective dielectric constants for benzene and hexane in Coulomb's law expression, we estimated the Coulomb stabilization energy for **2** to be 0.066 eV lower than that for **1**.[27] The resulting $\Delta_r G$ values are in qualitative agreement with the experimental data. The difference in the value of $\Delta_{vac}G$ for solutes **1** and **2** was also estimated by treating $\Delta_{vac}G$ as an adjustable parameter,

(24) Gu, Y.; Kumar, K.; Lin, A.; Read, I.; Zimmt, M. B.; Waldeck, D. H. *J. Photochem. Photobiol., A* **1997**, *105*, 189.

(25) (a) Paddon-Row, M. N.; Oliver, A. M.; Warman, J. M.; Smit, K. J.; de Haas, M. P.; Oevering, H.; Verhoeven, J. W. *J. Phys. Chem.* **1988**, *92*, 6958. (b) Warman, J. M.; Smit, K. J.; de Haas, M. P.; Jonker, S. A.; Paddon-Row, M. N.; Oliver, A. M.; Kroon, J.; Oevering, H.; Verhoeven, J. W. *J. Phys. Chem.* **1991**, *95*, 1979.

(26) The polarizabilities of the molecules were obtained using the HF/3-21+G method and a "divide and conquer" approach. Calculations were performed for analogues of **1** and **2** that did not contain the phenyl substituents on the naphthalene, nor the four CH$_2$OCH$_3$ groups on the bridge. This calculation yielded values of 73 Å^3 for the analogue of **1** and 70 Å^3 for the analogue of **2**. Independent calculations for the phenyl and ether substituents gave 9 and 4 Å^3, respectively. The polarizability of **1** and **2** were obtained by assuming that the polarizabilities of these components were additive and yielded 107 Å^3 for **1** and 103 Å^3 for **2**. A comparison of calculated polarizabilities for a range of molecules whose polarizabilities are known indicated that the calculation systematically underestimated the polarizability by a factor of 0.83. Correction by this factor gives 128 Å^3 for **1** and 124 Å^3 for **2**.

(27) The molecular moiety's polarizability was used to estimate the effective dielectric constant of the molecular cleft through the Clausius−Mossatti relationship. The polarizability perpendicular to the propyl group's long axis was taken to be 5.7 Å^3, and the polarizability perpendicular to the phenyl axis was taken to be 7.4 Å^3. The polarizabilities were taken from: Ma, B.; Lii, J.-H.; Allinger, N. L. *J. Comput. Chem.* **2000**, *21*, 813. The cleft volume was estimated to be 100 Å^3. This simple calculation predicts a shift in the reaction free energy between compounds **1** and **2** that is similar to the observed difference.

Table 3. Best Fit $|V|$ and λ_o(295 K) Values for the Aromatic Systems

system	$|V|$, cm^{-1}	λ_o(295 K) in toluene, eV	λ_o(295 K) in mesitylene, eV
1	168	0.73	0.69
2	46	0.59	0.56

which was constrained by fitting the experimental Gibbs free energy data from predictions derived using the molecular solvation model. The best fit difference of 0.045 eV is quite close to the observed difference and that which is estimated. The table in Appendix A gives the predicted $\Delta_r G$ values and lists the contributions from the different terms in eq 5.

With a parametrization of the internal reorganization energy parameters (λ_i and ν) and the reaction free energy ($\Delta_r G$) in hand, it is possible to fit the temperature-dependent rate data to the form of eq 1 and obtain values for the electronic coupling parameter $|V|$ and the solvent reorganization energy λ_o. This analysis would be straightforward if $|V|$ and λ_o were known to be temperature independent. Although $|V|$ is likely to satisfy this approximation, the solvent reorganization energy is expected to be temperature dependent because the solvation of the solute by the solvent is temperature dependent. For this reason, the molecular model that is parametrized to the reaction free energy data is used to treat the temperature dependence of the solvent reorganization energy. The temperature-dependent rate constant data can then be used to extract the best fit parameters for the electronic coupling parameter $|V|$ and the solvent reorganization energy at 295 K, λ_o(295 K).

Determination of λ_o

The outer-sphere reorganization energy is also calculated using this molecular solvation model. The reorganization energy is written as a sum of three components

$$\lambda_o = \lambda_p + \lambda_{ind} + \lambda_{disp} \qquad (6)$$

where λ_p accounts for solvent reorganization arising from the solvent dipole and quadrupole moments, λ_{ind} is the contribution from induction forces, and λ_{disp} accounts for the dispersion interactions. The model treats the solute as a dipolar, polarizable sphere and finds the reorganization energy; see the Appendix and earlier work[14,15] for further details. The Appendix also provides the values of the reaction free energy and the reorganization energy that are predicted by the model. It is well appreciated that continuum calculations are unreliable in nonpolar solvents. More importantly, the continuum theory fails to predict the temperature dependence of λ_o, that is, the sign of $d\lambda_o/dT$, even in polar systems, whereas the molecular model predicts the correct temperature dependence.[10a] The continuum model incorporates only the temperature dependence of molecular rotation, whereas the molecular model includes both translational and rotational degrees of freedom so that the temperature dependence of the reorganization energy is more faithfully reproduced. For these reasons, the molecular model is used to calculate $d\lambda_o/dT$, and an adjustable offset is used to fit the experimental data. The best fit λ_o(295 K) values are reported in Tables 3 and 4.

Determination of the Electronic Coupling, $|V|$

Using the values obtained for λ_i, ν, $\Delta_r G$, and $d\lambda_o/dT$, it is possible to fit the temperature-dependent rate data to eq 1 and

Table 4. Free Energy and Reorganization Energies for **1** and **2** in the More Polar Solvents

solvent	$\Delta_r G^a$(295 K), eV		λ_o(295 K), eV	
	1	**2**	**1**	**2**
THF	−0.37	−0.42	1.13	1.09
CH$_2$Cl$_2$	−0.37	−0.42	1.20	1.16
CH$_3$CN	−0.52	−0.57	1.50	1.50

^{a} The reaction free energy was calculated using the molecular model for solvation. Details may be found in the text and in the Appendix.
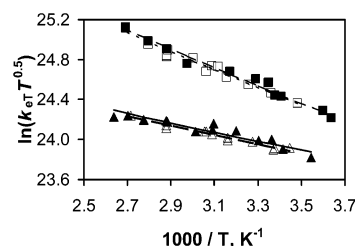

Figure 3. Experimental rate data (k_{for}) are plotted versus $1/T$, for **1** in toluene ($\square$), **1** in mesitylene ($\blacksquare$), **2** in toluene ($\triangle$), and **2** in mesitylene ($\blacktriangle$). The lines represent the best fits to eq **1**; see text for details.
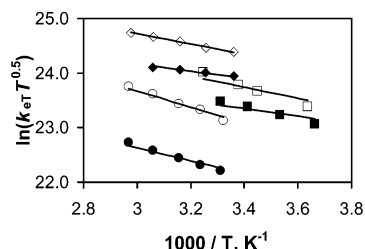
Figure 4. Experimental rate data (k_{for}) are plotted versus $1/T$, for **1** in CH$_3$CN ($\bigcirc$), CH$_2$Cl$_2$ ($\square$), and THF ($\diamond$) and **2** in CH$_3$CN ($\bullet$), CH$_2$Cl$_2$ ($\blacksquare$), and THF ($\blacklozenge$). The lines represent the best fits to eq 1; see text for details.

obtain electronic coupling $|V|$ and λ_o(295 K) values. For these systems, λ_i was taken to be 0.63 eV, and ν was taken to be 1600 cm^{-1}. The fitting was performed using $\Delta_r G(T)$ and $d\lambda_o/dT$ values predicted by the molecular model. Figures 3 and 4 show fits of the model to the rate data for **1** and **2** in toluene and mesitylene as well as three more polar solvents, CH$_2$Cl$_2$, THF, and acetonitrile. The rate data for **1** and **2** in the latter three solvents were reported earlier,[13] but until now a quantitative analysis of the data has not been reported. The rate data were fit to eq 1 by adjusting λ_o(295 K) in each solute−solvent system and adjusting the electronic coupling of the solute. Clearly, the fit quality is excellent.

The values obtained for $|V|$ and λ_o are reported in Tables 3 and 4. The electronic coupling is not dependent on the solvent, and the value obtained for **1** is 3 to 4 times larger than the value obtained for **2**, 168 cm^{-1} versus 46 cm^{-1}. From eq 1, a 3- to 4-fold increase in the electronic coupling should give rise to a 9- to 16-fold increase in the rate constants. However, the magnitude of the *FCWDS* term, arising from the differing $\Delta_r G(T)$ data, also changes for **1** and **2**, and this change partially counteracts the effect from the change in $|V|$. The best fit λ_o values, evaluated at 295 K, are also reported. From simple continuum arguments, the solvent reorganization energy is expected to be larger for the solvent with the more dipolar character, and this expectation is verified for both **1** and **2** (see Tables 3 and 4). In addition, the reorganization energy for **1** is found to be a bit higher than that for **2** in most of the solvents, which may indicate a small difference in the effective molecular
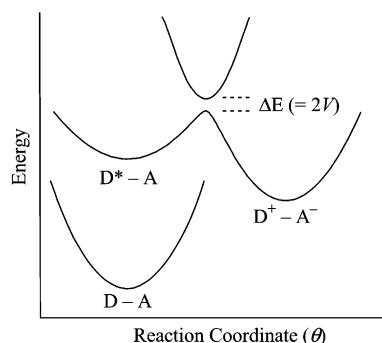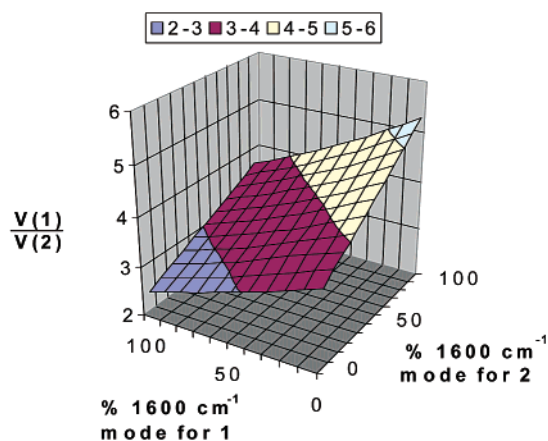
Figure 5. A schematic of the potential energy surface for photoinduced electron transfer is shown here. D—A is the ground-state surface, D*—A is the locally excited-state surface, and D^+-A^- is the CS-state surface. At the avoided crossing, the energy gap beteen the locally excited and CS states, ΔE, is twice the electronic coupling matrix element for electron transfer, $|V|$.

Figure 6. The internal reorganization energy is systematically partitioned between a 1600 and a 990 cm^{-1} mode. The three-dimensional plot demonstrates the ratio of $|V|$ that is obtained between **1** and **2** for a given percentage of 1600 cm^{-1} mode. The lower frequency model corresponds to a pyramidalization of the cyanoethylene acceptor group, whereas the higher frequency mode corresponds to a skeletal breathing mode of the naphthalene donor.

volume or dipole moment between the molecules. The dependence of the electronic coupling ratio ($|V(\mathbf{1})|/|V(\mathbf{2})|$) on the value of the solvent reorganization energy was analyzed in a systematic manner, and the electronic coupling of **1** was found to be larger than that of **2** for all reasonable reorganization energies. Details of this analysis are provided in the Supporting Information, which contains contour plots of $|V(\mathbf{1})|/|V(\mathbf{2})|$ and χ^2 as a function of λ_o, and plots such as that shown in Figure 3 under different fitting constraints.

Within the context of a two-state model, the electronic coupling matrix element $|V|$ may be taken to be one-half of the energy gap at the avoided crossing of the two adiabatic electronic states, in this case being the locally excited and the CS states (i.e., $\Delta E = 2V$), as shown in Figure 5. To determine if the electronic coupling between the DMN and DCV groups is in fact mediated by the substituent on the central imide group, or whether the coupling proceeds mainly via a through-bond mechanism,[28] ΔE was calculated for model systems based on the *N*-phenyl system, **7**, using the CIS method. Given the size of these systems, two approximations were made to make the analysis computationally feasible. First, the model system **7′** was created, which, while possessing the same geometry as the CS state of the *N*-phenyl imide, **7**, has a hydrogen atom in place of the phenyl group (with an N—H bond length of 1.01 Å).[29] Second, it was assumed that the reaction coordinate for the electron transfer in **7** (and **7′**) is the DCV pyramidalization angle, θ, and that all other geometrical parameters are frozen. This assumption was deemed reasonable because exploratory calculations on **7** revealed that the electron-transfer process is very sensitive to the magnitude of θ but not other geometrical features. Thus, for both **7** and **7′**, a series of CIS/3-21G single point energy calculations was carried out in which θ was varied until the energy gap between the locally excited state and the CS state reached a minimum value which was then equated to twice the value of the electronic coupling, $|V|$.

In the case of **7**, the avoided crossing is encountered when the DCV is only slightly pyramidalized, with $\theta = 12°$. The

electronic coupling, $|V|$, at this point is 16 cm^{-1}. In the case of **7′**, the avoided crossing occurs at a slightly larger pyramidalization angle of $\theta = 17.5°$, with $|V|$ equal to 5 cm^{-1}. Thus, $|V|$ for **7′** is significantly smaller, by a factor of 3, than that calculated for **7**. While the predicted magnitude of $|V|$ for **7** is substantially smaller than that estimated for **1**, from experimental data, the calculations correctly predict a 3- to 4-fold enhancement of the electronic coupling that arises from the presence of the aromatic ring in the molecular cavity of **7**, compared to **7′**. The enhancement in the magnitude of $|V|$ is, no doubt, caused by a superexchange mechanism. These computational results indicate that the central R group is important in mediating the coupling between the DMN and the DCV groups and that a U-shaped system provides a controlled way to analyze effects that different solvents may have upon inter- and intramolecular electron-transfer processes.

The magnitude of the electronic coupling that is extracted from experimental data depends strongly on the value of other parameters in eq 1, in particular, the reorganization energies, the effective frequency, and the free energy. The analysis in mesitylene and toluene uses the experimental free energy and adjusts the outer-sphere reorganization energy along with the electronic coupling to fit the rate data. The impact of the modeling for the inner-sphere reorganization energy with a single effective quantum mode was assessed by considering a two-mode model (vide supra). The use of a two-mode model generated results that are consistent with that found from the single-mode model; that is, the electronic coupling in **1** is significantly larger than that in **2**. Figure 6 shows how the ratio of electronic coupling magnitudes changes when the partitioning of the internal reorganization energy between the 1600 cm^{-1} mode and the 990 cm^{-1} mode is changed for each of the species **1** and **2**. This analysis shows that the ratio can change over the range from 2.5 to 5, depending on the details of the mode partitioning, but that the electronic coupling in **1** is always larger than that in **2**. In addition, when the partitioning of internal reorganization energy between the vibrational modes is similar in the two compounds (represented by the diagonal in the horizontal plane of the graph that goes from the origin of (0%,0% − a 900 cm^{-1} quantum mode in each compound) to

(28) (a) Hoffmann, R. *Acc. Chem. Res.* **1971**, *4*, 1. (b) Paddon-Row, M. N. *Acc. Chem. Res.* **1982**, *15*, 245. (c) Paddon-Row, M. N. In *Electron-Transfer In Chemistry*; Balzani, V., Ed.; Wiley-VCH: Weinheim, 2001; Vol. 3, Part 2, Chapter 1, p 179.

(29) The N—H system, **4**, was not used for these calculations because, given the approximations made, the modified system, **7′**, provides a better comparison to **7** for the influence that the phenyl group has upon the DMN—DCV coupling.

Table 5. Individual Contributions to $\Delta_r G$ and λ_0 for **1**[a]

T (K)	$\Delta_{dq,i}G^{(1)}$	$\Delta_i G^{(2)}$	$\Delta_{disp}G$	$\Delta_r G$	λ_p	λ_{ind}	λ_{disp}	λ_o
				Toluene				
287.15	-2.41×10^{-01}	-1.16×10^{-02}	-2.91×10^{-02}	-1.23×10^{-01}	5.60×10^{-02}	1.07×10^{-02}	4.75×10^{-04}	6.72×10^{-02}
297.55	-2.35×10^{-01}	-1.07×10^{-02}	-2.86×10^{-02}	-1.16×10^{-01}	5.37×10^{-02}	9.91×10^{-03}	4.48×10^{-04}	6.40×10^{-02}
298.75	-2.35×10^{-01}	-1.07×10^{-02}	-2.86×10^{-02}	-1.15×10^{-01}	5.34×10^{-02}	9.83×10^{-03}	4.45×10^{-04}	6.37×10^{-02}
307.15	-2.30×10^{-01}	-1.00×10^{-02}	-2.82×10^{-02}	-1.09×10^{-01}	5.16×10^{-02}	9.27×10^{-03}	4.25×10^{-04}	6.13×10^{-02}
316.95	-2.25×10^{-01}	-9.40×10^{-03}	-2.78×10^{-02}	-1.03×10^{-01}	4.96×10^{-02}	8.67×10^{-03}	4.03×10^{-04}	5.86×10^{-02}
320.85	-2.23×10^{-01}	-9.15×10^{-03}	-2.76×10^{-02}	-1.01×10^{-01}	4.88×10^{-02}	8.44×10^{-03}	3.95×10^{-04}	5.76×10^{-02}
323.85	-2.21×10^{-01}	-8.97×10^{-03}	-2.74×10^{-02}	-9.88×10^{-02}	4.82×10^{-02}	8.27×10^{-03}	3.88×10^{-04}	5.69×10^{-02}
326.65	-2.20×10^{-01}	-8.80×10^{-03}	-2.73×10^{-02}	-9.71×10^{-02}	4.77×10^{-02}	8.12×10^{-03}	3.83×10^{-04}	5.62×10^{-02}
333.15	-2.17×10^{-01}	-8.42×10^{-03}	-2.70×10^{-02}	-9.32×10^{-02}	4.64×10^{-02}	7.77×10^{-03}	3.70×10^{-04}	5.46×10^{-02}
346.55	-2.10×10^{-01}	-7.70×10^{-03}	-2.65×10^{-02}	-8.55×10^{-02}	4.40×10^{-02}	7.11×10^{-03}	3.45×10^{-04}	5.15×10^{-02}
346.95	-2.10×10^{-01}	-7.68×10^{-03}	-2.64×10^{-02}	-8.53×10^{-02}	4.39×10^{-02}	7.09×10^{-03}	3.44×10^{-04}	5.14×10^{-02}
347.05	-2.10×10^{-01}	-7.68×10^{-03}	-2.64×10^{-02}	-8.52×10^{-02}	4.39×10^{-02}	7.08×10^{-03}	3.44×10^{-04}	5.14×10^{-02}
357.75	-2.05×10^{-01}	-7.16×10^{-03}	-2.60×10^{-02}	-7.93×10^{-02}	4.21×10^{-02}	6.60×10^{-03}	3.26×10^{-04}	4.90×10^{-02}
371.45	-1.99×10^{-01}	-6.54×10^{-03}	-2.54×10^{-02}	-7.20×10^{-02}	3.99×10^{-02}	6.04×10^{-03}	3.05×10^{-04}	4.62×10^{-02}
371.55	-1.99×10^{-01}	-6.54×10^{-03}	-2.54×10^{-02}	-7.19×10^{-02}	3.99×10^{-02}	6.03×10^{-03}	3.04×10^{-04}	4.62×10^{-02}
				Mesitylene				
274.95	-2.07×10^{-01}	-1.40×10^{-02}	-4.09×10^{-02}	-1.03×10^{-01}	3.35×10^{-02}	1.29×10^{-02}	1.16×10^{-03}	4.75×10^{-02}
277.85	-2.06×10^{-01}	-1.37×10^{-02}	-4.07×10^{-02}	-1.01×10^{-01}	3.31×10^{-02}	1.26×10^{-02}	1.14×10^{-03}	4.68×10^{-02}
293.55	-1.99×10^{-01}	-1.23×10^{-02}	-3.98×10^{-02}	-9.19×10^{-02}	3.07×10^{-02}	1.14×10^{-02}	1.04×10^{-03}	4.31×10^{-02}
295.95	-1.98×10^{-01}	-1.21×10^{-02}	-3.96×10^{-02}	-9.05×10^{-02}	3.04×10^{-02}	1.12×10^{-02}	1.02×10^{-03}	4.26×10^{-02}
298.45	-1.97×10^{-01}	-1.19×10^{-02}	-3.95×10^{-02}	-8.91×10^{-02}	3.00×10^{-02}	1.10×10^{-02}	1.01×10^{-03}	4.21×10^{-02}
304	-1.94×10^{-01}	-1.15×10^{-02}	-3.91×10^{-02}	-8.60×10^{-02}	2.93×10^{-02}	1.06×10^{-02}	9.78×10^{-04}	4.09×10^{-02}
315.35	-1.90×10^{-01}	-1.07×10^{-02}	-3.84×10^{-02}	-7.99×10^{-02}	2.78×10^{-02}	9.85×10^{-03}	9.17×10^{-04}	3.86×10^{-02}
336.35	-1.82×10^{-01}	-9.35×10^{-03}	-3.72×10^{-02}	-6.92×10^{-02}	2.54×10^{-02}	8.63×10^{-03}	8.18×10^{-04}	3.48×10^{-02}
347.05	-1.78×10^{-01}	-8.75×10^{-03}	-3.65×10^{-02}	-6.40×10^{-02}	2.42×10^{-02}	8.07×10^{-03}	7.73×10^{-04}	3.30×10^{-02}
357.75	-1.74×10^{-01}	-8.20×10^{-03}	-3.59×10^{-02}	-5.89×10^{-02}	2.31×10^{-02}	7.56×10^{-03}	7.31×10^{-04}	3.14×10^{-02}
371.55	-1.69×10^{-01}	-7.54×10^{-03}	-3.51×10^{-02}	-5.27×10^{-02}	2.18×10^{-02}	6.96×10^{-03}	6.81×10^{-04}	2.94×10^{-02}
				THF				
297.5	-4.92×10^{-01}	-5.36×10^{-03}	-3.27×10^{-02}	-3.71×10^{-01}	2.21×10^{-01}	4.95×10^{-03}	4.88×10^{-04}	2.26×10^{-01}
307.1	-4.83×10^{-01}	-5.00×10^{-03}	-3.23×10^{-02}	-3.61×10^{-01}	2.16×10^{-01}	4.61×10^{-03}	4.63×10^{-04}	2.21×10^{-01}
316.4	-4.73×10^{-01}	-4.67×10^{-03}	-3.18×10^{-02}	-3.51×10^{-01}	2.11×10^{-01}	4.30×10^{-03}	4.41×10^{-04}	2.16×10^{-01}
326.7	-4.64×10^{-01}	-4.33×10^{-03}	-3.14×10^{-02}	-3.40×10^{-01}	2.06×10^{-01}	3.99×10^{-03}	4.18×10^{-04}	2.10×10^{-01}
336	-4.55×10^{-01}	-4.05×10^{-03}	-3.09×10^{-02}	-3.31×10^{-01}	2.01×10^{-01}	3.74×10^{-03}	3.99×10^{-04}	2.05×10^{-01}
				Acetonitrile				
301	-6.52×10^{-01}	-1.38×10^{-02}	-2.01×10^{-02}	-5.27×10^{-01}	3.49×10^{-01}	1.28×10^{-02}	1.38×10^{-04}	3.62×10^{-01}
309	-6.47×10^{-01}	-1.37×10^{-02}	-1.98×10^{-02}	-5.21×10^{-01}	3.47×10^{-01}	1.27×10^{-02}	1.32×10^{-04}	3.59×10^{-01}
317	-6.41×10^{-01}	-1.36×10^{-02}	-1.96×10^{-02}	-5.16×10^{-01}	3.44×10^{-01}	1.26×10^{-02}	1.26×10^{-04}	3.57×10^{-01}
327	-6.35×10^{-01}	-1.35×10^{-02}	-1.92×10^{-02}	-5.08×10^{-01}	3.41×10^{-01}	1.24×10^{-02}	1.19×10^{-04}	3.54×10^{-01}
337	-6.28×10^{-01}	-1.34×10^{-02}	-1.88×10^{-02}	-5.01×10^{-01}	3.38×10^{-01}	1.23×10^{-02}	1.13×10^{-04}	3.50×10^{-01}
				Dichloromethane				
275	-5.29×10^{-01}	-6.37×10^{-03}	-2.31×10^{-02}	-3.99×10^{-01}	2.51×10^{-01}	5.88×10^{-03}	2.18×10^{-04}	2.57×10^{-01}
290	-5.13×10^{-01}	-5.73×10^{-03}	-2.24×10^{-02}	-3.82×10^{-01}	2.43×10^{-01}	5.28×10^{-03}	1.98×10^{-04}	2.49×10^{-01}
296	-5.06×10^{-01}	-5.49×10^{-03}	-2.21×10^{-02}	-3.75×10^{-01}	2.40×10^{-01}	5.07×10^{-03}	1.91×10^{-04}	2.45×10^{-01}
308	-4.94×10^{-01}	-5.06×10^{-03}	-2.16×10^{-02}	-3.61×10^{-01}	2.33×10^{-01}	4.66×10^{-03}	1.78×10^{-04}	2.38×10^{-01}

[a] All values listed are in eV.

the point at (100%,100% − a 1600 cm^{-1} quantum mode in each compound)), the ratio does not change dramatically. To the extent that the donor and acceptor groups rather than the pendant moiety control the partitioning, this observation suggests that the ratio of ca. 3 for the electronic coupling magnitudes is robust with respect to the modeling for the internal reorganization energy.

Conclusions

This work presents electron-transfer rate data and computational results that demonstrate efficient electron tunneling through a pendant moiety located in the *line-of-sight* between electron donor and acceptor groups. The electron-transfer rates for compounds **1** and **2** were compared with that of control molecule **8** to demonstrate that the electron transfer proceeds through the pendant moiety, rather than the covalent bridge. The experimentally determined reaction free energy for **1** in toluene and mesitylene and **2** in mesitylene was used to calibrate a molecular-based model for solvation. This model and charge-transfer spectra were used to define the reorganization energy and free energy parameters for electron transfer of **1** and **2** in the five solvents studied. By combining the knowledge of these parameters with the temperature-dependent rate data, it was possible to experimentally determine the electronic coupling for these two compounds in the solvents. Compound **1** was found to have an electronic coupling that is 3 to 4 times larger than that of compound **2**. The dependence of the empirically derived electronic coupling values on the reorganization energy parameters was evaluated in detail (see Discussion and Supporting Information). Also, the electronic couplings for the compounds were found to be independent of the solvent. The difference in electronic coupling values reflects the more efficient tunneling through the aromatic moiety of **1** than the alkyl moiety of **2**. The absolute values of the experimentally derived electronic coupling values obtained for **1** and **2** were shown to be larger than those calculated by ab initio molecular orbital theory for

Table 6. Individual Contributions to $\Delta_r G$ and λ_o for **2**[a]

T (K)	$\Delta_{dq,i}G^{(1)}$	$\Delta_i G^{(2)}$	$\Delta_{disp}G$	$\Delta_r G$	λ_p	λ_{ind}	λ_{disp}	λ_o
				Toluene				
290.25	-2.38×10^{-01}	-1.12×10^{-02}	-2.89×10^{-02}	-1.19×10^{-01}	5.49×10^{-02}	1.04×10^{-02}	4.67×10^{-04}	6.58×10^{-02}
296.15	-2.35×10^{-01}	-1.08×10^{-02}	-2.87×10^{-02}	-1.15×10^{-01}	5.36×10^{-02}	9.96×10^{-03}	4.52×10^{-04}	6.40×10^{-02}
296.65	-2.35×10^{-01}	-1.08×10^{-02}	-2.86×10^{-02}	-1.15×10^{-01}	5.35×10^{-02}	9.92×10^{-03}	4.50×10^{-04}	6.39×10^{-02}
305.35	-2.30×10^{-01}	-1.01×10^{-02}	-2.83×10^{-02}	-1.09×10^{-01}	5.17×10^{-02}	9.34×10^{-03}	4.29×10^{-04}	6.14×10^{-02}
316.3	-2.24×10^{-01}	-9.39×10^{-03}	-2.78×10^{-02}	-1.03×10^{-01}	4.94×10^{-02}	8.66×10^{-03}	4.04×10^{-04}	5.85×10^{-02}
316.45	-2.24×10^{-01}	-9.38×10^{-03}	-2.78×10^{-02}	-1.02×10^{-01}	4.94×10^{-02}	8.65×10^{-03}	4.04×10^{-04}	5.84×10^{-02}
323.75	-2.21×10^{-01}	-8.93×10^{-03}	-2.75×10^{-02}	-9.80×10^{-02}	4.79×10^{-02}	8.24×10^{-03}	3.89×10^{-04}	5.66×10^{-02}
326.65	-2.19×10^{-01}	-8.76×10^{-03}	-2.73×10^{-02}	-9.63×10^{-02}	4.74×10^{-02}	8.08×10^{-03}	3.83×10^{-04}	5.58×10^{-02}
327.5	-2.19×10^{-01}	-8.71×10^{-03}	-2.73×10^{-02}	-9.58×10^{-02}	4.72×10^{-02}	8.03×10^{-03}	3.81×10^{-04}	5.56×10^{-02}
347.55	-2.09×10^{-01}	-7.62×10^{-03}	-2.64×10^{-02}	-8.42×10^{-02}	4.36×10^{-02}	7.03×10^{-03}	3.43×10^{-04}	5.10×10^{-02}
347.55	-2.09×10^{-01}	-7.62×10^{-03}	-2.64×10^{-02}	-8.42×10^{-02}	4.36×10^{-02}	7.03×10^{-03}	3.43×10^{-04}	5.10×10^{-02}
368.3	-2.00×10^{-01}	-6.65×10^{-03}	-2.55×10^{-02}	-7.29×10^{-02}	4.02×10^{-02}	6.13×10^{-03}	3.09×10^{-04}	4.66×10^{-02}
				Mesitylene				
282.15	-2.03×10^{-01}	-1.32×10^{-02}	-4.05×10^{-02}	-9.78×10^{-02}	3.22×10^{-02}	1.22×10^{-02}	1.11×10^{-03}	4.55×10^{-02}
292.85	-1.99×10^{-01}	-1.23×10^{-02}	-3.98×10^{-02}	-9.16×10^{-02}	3.07×10^{-02}	1.14×10^{-02}	1.04×10^{-03}	4.31×10^{-02}
297.45	-1.97×10^{-01}	-1.19×10^{-02}	-3.95×10^{-02}	-8.90×10^{-02}	3.00×10^{-02}	1.10×10^{-02}	1.01×10^{-03}	4.20×10^{-02}
302.75	-1.94×10^{-01}	-1.15×10^{-02}	-3.92×10^{-02}	-8.60×10^{-02}	2.93×10^{-02}	1.06×10^{-02}	9.85×10^{-04}	4.09×10^{-02}
312.55	-1.90×10^{-01}	-1.08×10^{-02}	-3.86×10^{-02}	-8.07×10^{-02}	2.80×10^{-02}	9.98×10^{-03}	9.32×10^{-04}	3.89×10^{-02}
323.05	-1.86×10^{-01}	-1.01×10^{-02}	-3.80×10^{-02}	-7.52×10^{-02}	2.67×10^{-02}	9.34×10^{-03}	8.79×10^{-04}	3.70×10^{-02}
323.65	-1.86×10^{-01}	-1.01×10^{-02}	-3.79×10^{-02}	-7.49×10^{-02}	2.67×10^{-02}	9.30×10^{-03}	8.76×10^{-04}	3.68×10^{-02}
331.75	-1.83×10^{-01}	-9.58×10^{-03}	-3.74×10^{-02}	-7.09×10^{-02}	2.57×10^{-02}	8.84×10^{-03}	8.38×10^{-04}	3.54×10^{-02}
346.65	-1.77×10^{-01}	-8.73×10^{-03}	-3.66×10^{-02}	-6.36×10^{-02}	2.41×10^{-02}	8.06×10^{-03}	7.74×10^{-04}	3.29×10^{-02}
347.45	-1.77×10^{-01}	-8.69×10^{-03}	-3.65×10^{-02}	-6.32×10^{-02}	2.40×10^{-02}	8.02×10^{-03}	7.71×10^{-04}	3.28×10^{-02}
360.25	-1.73×10^{-01}	-8.04×10^{-03}	-3.58×10^{-02}	-5.73×10^{-02}	2.27×10^{-02}	7.41×10^{-03}	7.21×10^{-04}	3.09×10^{-02}
360.35	-1.73×10^{-01}	-8.03×10^{-03}	-3.58×10^{-02}	-5.72×10^{-02}	2.27×10^{-02}	7.41×10^{-03}	7.21×10^{-04}	3.09×10^{-02}
370.15	-1.69×10^{-01}	-7.57×10^{-03}	-3.52×10^{-02}	-5.28×10^{-02}	2.18×10^{-02}	6.98×10^{-03}	6.86×10^{-04}	2.95×10^{-02}
379.25	-1.66×10^{-01}	-7.17×10^{-03}	-3.47×10^{-02}	-4.88×10^{-02}	2.10×10^{-02}	6.61×10^{-03}	6.55×10^{-04}	2.82×10^{-02}
				THF				
297.5	-4.88×10^{-01}	-5.34×10^{-03}	-3.27×10^{-02}	-3.67×10^{-01}	2.18×10^{-01}	4.93×10^{-03}	4.88×10^{-04}	2.24×10^{-01}
307.2	-4.79×10^{-01}	-4.97×10^{-03}	-3.23×10^{-02}	-3.57×10^{-01}	2.14×10^{-01}	4.58×10^{-03}	4.63×10^{-04}	2.19×10^{-01}
316.4	-4.70×10^{-01}	-4.65×10^{-03}	-3.18×10^{-02}	-3.47×10^{-01}	2.09×10^{-01}	4.29×10^{-03}	4.41×10^{-04}	2.14×10^{-01}
326.9	-4.60×10^{-01}	-4.30×10^{-03}	-3.13×10^{-02}	-3.37×10^{-01}	2.04×10^{-01}	3.97×10^{-03}	4.18×10^{-04}	2.08×10^{-01}
				Acetonitrile				
302	-6.45×10^{-01}	-1.38×10^{-02}	-2.01×10^{-02}	-5.20×10^{-01}	3.44×10^{-01}	1.27×10^{-02}	1.37×10^{-04}	3.57×10^{-01}
309	-6.40×10^{-01}	-1.37×10^{-02}	-1.98×10^{-02}	-5.15×10^{-01}	3.42×10^{-01}	1.26×10^{-02}	1.32×10^{-04}	3.55×10^{-01}
317	-6.35×10^{-01}	-1.36×10^{-02}	-1.96×10^{-02}	-5.09×10^{-01}	3.40×10^{-01}	1.25×10^{-02}	1.26×10^{-04}	3.53×10^{-01}
327	-6.28×10^{-01}	-1.34×10^{-02}	-1.92×10^{-02}	-5.02×10^{-01}	3.37×10^{-01}	1.24×10^{-02}	1.19×10^{-04}	3.49×10^{-01}
337	-6.22×10^{-01}	-1.33×10^{-02}	-1.88×10^{-02}	-4.95×10^{-01}	3.34×10^{-01}	1.23×10^{-02}	1.13×10^{-04}	3.46×10^{-01}
				Dichloromethane				
273	-5.27×10^{-01}	-6.43×10^{-03}	-2.31×10^{-02}	-3.97×10^{-01}	2.50×10^{-01}	5.93×10^{-03}	2.21×10^{-04}	2.56×10^{-01}
283	-5.16×10^{-01}	-5.99×10^{-03}	-2.27×10^{-02}	-3.86×10^{-01}	2.44×10^{-01}	5.52×10^{-03}	2.07×10^{-04}	2.50×10^{-01}
293	-5.05×10^{-01}	-5.58×10^{-03}	-2.22×10^{-02}	-3.74×10^{-01}	2.39×10^{-01}	5.15×10^{-03}	1.95×10^{-04}	2.44×10^{-01}
302	-4.96×10^{-01}	-5.24×10^{-03}	-2.18×10^{-02}	-3.64×10^{-01}	2.34×10^{-01}	4.84×10^{-03}	1.84×10^{-04}	2.39×10^{-01}

[a] All values listed are in eV.

analogues of **1** and **2**, but both agree that an aromatic group is better than a propyl group in mediating the electron-transfer process.

Appendix A

The molecular model for solvation in these electron-transfer systems has been discussed extensively in earlier work.[14] This model develops explicit expressions for the reaction free energy and the solvent reorganization energy.

The free energy of reaction is given by the sum of four terms in eq 5. The most significant contribution in these solvents comes from the $\Delta_{dq,i}G^{(1)}$ term given by

$$\Delta_{dq,i}G^{(1)} = -\frac{(m_e^2 - m_g^2)}{R_{eff}^3} f(y_d, y_q)\Psi^P(y_d, y_q) \quad \text{(A1)}$$

where m_i is the permanent dipole moment of the excited and ground electronic states, $f(y_d, y_q)$ renormalizes the solute dipole moment to account for its size and polarizability, R_{eff} is the effective solute radius, and $\Psi(y_d, y_q)$ is the polarity response function given by

$$\Psi^P(y_d, y_q) = \frac{\dfrac{y_d I_{0s}^{(2)} + y_q I_6^{(2)}}{I_{0s}^{(2)}}}{1 + \dfrac{y_d^2 \kappa_d I_{0s}^{(3)} + y_d y_q \kappa_{dq} I_{DDQ}^{(3)} + y_q^2 \kappa_q I_{DQQ}^{(3)}}{y_d I_{0s}^{(2)} + y_q I_6^{(2)}}} \quad \text{(A2)}$$

In this equation, the κ terms account for saturation of the dipolar response that arises from higher order interactions, and the I_{ij}

are polynomial representations of the two and three particle perturbation integrals. Their explicit form can be found elsewhere.[14,30]

The solvent reorganization energy is given by a sum of three terms in eq 6. The major contribution in the aromatic solvents comes from λ_p and is given by

$$\lambda_p = \frac{(m_e - m_g)^2}{R_{eff}^3} [f(y_d, y_q)\Psi^P(y_d, y_q) - f(y_e)\Psi^P(y_e)] \quad (A3)$$

where y_e is the reduced polarizability density of the solvent. The induction term λ_{ind} makes a small but relatively significant contribution to the overall reorganization energy in these solvents (see Tables 5 and 6) and is given by

$$\lambda_{ind} = \frac{(m_e^2 - m_g^2)^2 f(y_e)^2}{400 \text{ kT } \eta\sigma^6} \frac{(\epsilon_\infty - 1)^2}{(\epsilon_\infty + 2)^2} \left[3 + \frac{8}{3}(\epsilon_\infty - 1)^2\right] I_{0s}^{(4)} \quad (A4)$$

where η is the reduced packing density of the solvent molecules, σ is the solvent hard sphere diameter,[31] and ϵ_∞ is the solvent high-frequency dielectric constant. Previous work[14] indicated that the absolute values of λ_o predicted from the model are too small. Therefore, only its temperature dependence is used.

Supporting Information Available: Tables containing the Cartesian coordinates of all structures and rate constant data for **1** and **2** in all solvents as a function of temperature (PDF). This material is available free of charge via the Internet at http://pubs.acs.org.

JA025683S

(30) (a) Matyushov, D. V.; Schmid, R. *J. Chem. Phys.* **1996**, *105*, 4729. (b) Matyushov, D. V.; Ladanyi, B. M. *J. Chem. Phys.* **1999**, *110*, 994.

(31) Ben-Amotz, D.; Willis, K. G. *J. Phys. Chem.* **1993**, *97*, 7736.